Vibrational and thermodynamic properties of $MgSiO_3$ postperovskite

Jun Tsuchiya, Taku Tsuchiya, and Renata M. Wentzcovitch

Department of Chemical Engineering and Materials Science, Minnesota Supercomputing Institute for Digital Technology and Advanced Computation, University of Minnesota, Minneapolis, Minnesota, USA

Received 26 August 2004; revised 26 November 2004; accepted 13 December 2004; published 4 February 2005.

[1] Phonon dispersions and vibrational density of states of $MgSiO_3$ postperovskite, the new high-pressure phase of $MgSiO_3$ perovskite, are calculated as a function of pressure up to 180 GPa using density-functional perturbation theory. The calculated frequencies are then used to determine the thermal contribution to the Helmholtz free energy within the quasi-harmonic approximation. The equation of state and several thermodynamic properties of interest are derived and compared with those of perovskite. The overall thermodynamic properties of postperovskite are almost the same as those of perovskite under its stability conditions.

Citation: Tsuchiya, J., T. Tsuchiya, and R. M. Wentzcovitch (2005), Vibrational and thermodynamic properties of $MgSiO_3$ postperovskite, *J. Geophys. Res.*, *110*, B02204, doi:10.1029/2004JB003409.

1. Introduction

[2] The perovskite structure is one of the most popular crystal structures with ABO_3 composition. Among them, $MgSiO_3$ perovskite is considered to be the primary constituent of Earth's lower mantle. Recently, a high-pressure experiment reported a phase transformation in $MgSiO_3$ perovskite around 125 GPa and 2500 K [*Murakami et al.*, 2004]. Motivated by the drastic change in the experimental X-ray diffraction pattern, an early first principles investigation also found independently this structural transition, and determined the high-pressure crystal structure and the thermodynamic phase boundary [*Tsuchiya et al.*, 2004a] which reproduced approximately the thermodynamic conditions of the transformation. Another recent calculation seems to reach a similar conclusion [*Oganov and Ono*, 2004]. This transformation seems to take place at the conditions expected near the D″ seismic discontinuity above the core-mantle boundary (CMB). Several properties of this new found phase, together with the thermodynamic phase boundary, suggest that this transition might be the primary cause of the D″ discontinuity and that the postperovskite phase might be the most abundant mineral in the D″ region.

[3] $MgSiO_3$ postperovskite has the $CaIrO_3$-type crystal structure [*Hyde and Anderson*, 1989]. The transitions from *Pbnm*-perovskite to this type of crystal structure have recently been reported in other compounds [*Hirose et al.*, 2004; S. Ono et al., Phase transformation of perovskite structure in Fe_2O_3 at high pressures and high temperatures, submitted to American Mineralogist, 2004]. Postperovskite is a layered structure with highly anisotropic compressibility [*Tsuchiya et al.*, 2004a; *Iitaka et al.*, 2004; *Oganov and Ono*, 2004]. However, some elastic properties of this phase are different from those of typical layered minerals [*Tsuchiya et al.*, 2004b]. The postperovskite has considerably larger G than perovskite in the relevant pressure conditions. In order to better understand of basic properties of this phase and to further explore the importance of this phase as a D″ constituent, it is helpful to investigate its vibrational and thermodynamic properties. Comparison between the thermal expansivity, specific heat, and entropy of perovskite and of the postperovskite phase is essential to clarify the effect of this transformation on mantle dynamics also. However, experimental measurements of these properties under lower mantle conditions are not yet possible.

[4] Here we use the quasi-harmonic approximation (QHA) combined with first principles calculations of the vibrational density of states to compute the free energy of $MgSiO_3$ postperovskite and derive several thermodynamic properties of interest up to 180 GPa. We then compare with the same properties previously calculated in the perovskite phase [*Karki et al.*, 2000a, 2001].

2. Method

[5] Computations are performed within the local density approximation (LDA) [*Ceperley and Alder*, 1980; *Perdew and Zunger*, 1981] to density functional theory [*Hohenberg and Kohn*, 1964]. Calculational details are the same as in our previous work [*Tsuchiya et al.*, 2004a, 2004b] (Mg pseudopotential is generated by the method of von Barth and Car [*Karki et al.*, 2000b], whereas those for O and Si are by the method of *Troullier and Martins* [1991]). The plane wave cutoff is set at 70 Ry, and the Brillouin zone (BZ) of primitive lattice is sampled on $4 \times 4 \times 2$ Monkhorst-Pack mesh [*Monkhorst and Pack*, 1976]. The effects of using the larger cutoff and k points on the calculated properties are found to be insignificant.

0148-0227/05/2004JB003409$09.00

[6] The central quantity in the lattice-dynamical calculation is the dynamical matrix

$$\mathbf{D}^{\alpha\beta}_{\kappa\kappa'}(\mathbf{q}) = \frac{1}{\sqrt{m_\kappa m_{\kappa'}}} \sum_l \mathbf{\Phi}^{\alpha\beta}_{\kappa\kappa'}(0l) \exp[-i\mathbf{q}\cdot(\mathbf{x}_0 - \mathbf{x}_l)]. \quad (1)$$

Here the interatomic force constants $\mathbf{\Phi}^{\alpha\beta}_{\kappa\kappa'}(0l)$ include ionic and electronic contributions, the former being calculated from Evald sums and the latter being expressed as

$$\Phi^{\alpha\beta}_{\kappa\kappa'}(0l)_{el} = \int \left[\frac{\partial \rho(r)}{\partial u^\alpha_\kappa(0)} \frac{\partial V_{ion}(\mathbf{r})}{\partial u^\beta_{\kappa'}(l)} + \rho(\mathbf{r}) \frac{\partial^2 V_{ion}(\mathbf{r})}{\partial u^\alpha_\kappa(0) \partial u^\beta_{\kappa'}(l)} \right] d^3r, \quad (2)$$

where $\rho(\mathbf{r})$ is the electron density, $V_{ion}(\mathbf{r})$ is the ionic potential, and $\partial\rho(\mathbf{r})/\partial u^\alpha_\kappa$ (0) represents the density response of the system to a displacement of the κ atom in the reference cell (l = 0) along the α direction. This linear electron density response can be calculated self-consistently using density functional perturbation theory [*Baroni et al.*, 1987]. It is convenient to treat lattice displacements with a given periodicity $\mathbf{q}$, $u^\alpha_\kappa(l) = u^\alpha_\kappa(\mathbf{q})\exp[i\mathbf{q}\cdot\mathbf{x_l}]$, since the corresponding linear density response has the same periodicity and the dynamical matrix, $D^{\alpha\beta}_{\kappa\kappa'}(\mathbf{q})$, and the corresponding phonons can be determined directly at any wave vector $\mathbf{q}$ in the BZ without the need for supercells. At a given pressure (or volume), first the structure is fully optimized. Then the dynamical matrices are computed on regular 4 × 4 × 2 $\mathbf{q}$ grid, and are used for interpolation to obtain bulk phonon dispersions. For fitting the calculated energy-volume results, we used fourth-order finite strain equation of state and the samples volumes are at 0, 10, 20, 30, 40, 50, 60, 70, 80, 90, 100, 120, 150, 180 and 200 GPa for postperovskite and −10, 0, 30, 60, 90, 120, 150, and 180 GPa for perovskite. These methods have been successfully applied to MgO, SiO_2 polymorphs, $MgSiO_3$ perovskite, and ilmenite [*Karki et al.*, 2000b; *Tsuchiya et al.*, 2004c; *Karki et al.*, 2000a; *Wentzcovitch et al.*, 2004b].

[7] In polar semiconductors and insulators, phonons are coupled to macroscopic electric field in the long-wavelength limit. The nonanalytical contribution of the macroscopic electric field to the force constant tensor is given by

$$\frac{4\pi e^2}{V} \frac{(\mathbf{q}\cdot\mathbf{Z}^*_\kappa)_\alpha (\mathbf{q}\cdot\mathbf{Z}^*_{\kappa'})_\beta}{\mathbf{q}\cdot\varepsilon_\infty\cdot\mathbf{q}}, \quad (3)$$

where the tensors $\mathbf{Z}^*$ and ε_∞ are, the Born effective charges and macroscopic high-frequency static dielectric constant which are calculated self-consistently, respectively [*Baroni et al.*, 2001].

[8] In order to assess the mechanical stability of postperovskite, we applied the Born stability criteria [*Born and Huang*, 1954]. The Born stability criteria for an orthorhombic system are

$$B_{1,ii} = c_{ii} > 0 \qquad (i = 1-6), \quad (4)$$

$$B_{2,ij} = \begin{vmatrix} c_{ii} & c_{ij} \\ c_{ji} & c_{jj} \end{vmatrix} > 0 \qquad (ij = \{23\},\{31\},\text{or}\{12\}), \quad (5)$$

$$B_3 = \begin{vmatrix} c_{11} & c_{12} & c_{13} \\ c_{21} & c_{22} & c_{23} \\ c_{31} & c_{32} & c_{33} \end{vmatrix} > 0. \quad (6)$$

3. Results and Discussion

3.1. Vibrational Properties

[9] The postperovskite structure has base-centered orthorhombic structure with space group *Cmcm*. In this structure, the SiO_3 layers, containing edge shearing SiO_6 octahedra columns connected by octahedral apices, are intercalated by Mg ions. It has two formulae unit per *Cmcm* primitive cell (monoclinic, Z = 2) so there are 30 vibrational modes at any point in the BZ.

[10] Dynamical matrices are computed at 14 wave ($\mathbf{q}$) vectors in the BZ of the primitive cell of postperovskite (4 × 4 × 2 $\mathbf{q}$ grid without shift). We interpolated dynamical matrices to obtain the bulk phonon dispersions. The predicted dispersion curves along several symmetry directions and vibrational density of states (VDoS) at 0 and 120 GPa are shown in Figure 1. Though 0 GPa is obviously outside of its stability fields, these results are informative and indicative of the mechanical/vibrational stability of this phase. Under decompression the lowest acoustic branch starts drooping down around the Y point of the BZ (Figure 1a). This behavior is associated with the easier elongation of b axis under decompression.

[11] The diagonal components of the dielectric tensor are 3.53, 3.22, and 3.24 at zero pressure, and 3.27, 3.04, and 3.03 at 120 GPa. Born effective charges for Mg are close to the formal ionic charges of magnitudes equal to 2 and are weakly anisotropic: Z^*[Mg] = (2.00, 2.36, 2.13) at zero pressure and Z^*[Mg] = (1.85, 2.14, 2.00) at 120 GPa. However, those for Si and O are very anisotropic: Z^*[Si] = (3.98, 2.93, 3.60), Z^*[O(1)] = (−1.45, −1.55, −2.50), and Z^*[O(2)] = (−2.26, −1.87, −1.62) at zero pressure, and Z^*[Si] = (3.79, 2.99, 3.51), Z^*[O(1)] = (−1.49, −1.55, −2.34), and Z^*[O(2)] = (−2.08, −1.79, −1.59) at 120 GPa.

3.2. Postperovskite Stability

[12] The phonon dispersions displayed in Figure 1 reveal an interesting fact about postperovskite. Although there is an acoustic branch that softens under decompression, at 0 GPa all phonons are still stable. This type of acoustic phonon softening is typical of materials that amorphize under decompression (or compression), such as α-quartz [*Chaplot and Sikka*, 1993] or ice VIII [*Umemoto and Wentzcovitch*, 2004]. The frequencies along this branch (except around Γ), are in the range of 100 cm^{-1}, i.e., ∼140 K. This means that below this typical temperature these phonons are not very populated and therefore postperovskite may be retrieved metastably at 0 GPa, unless there is some nonobvious elastic instability.

[13] Here we use the elastic constants previously obtained [*Tsuchiya et al.*, 2004b] to inspect the Born stability criteria of postperovskite under decompression. Figure 2 shows that all the stability criteria decrease consistently under decompression, pointing to an increasing tendency toward mechanical instability under decompression. We could not get enough convergence of postperovskite structure at negative pressure. However, at 0 GPa these criteria are still positively

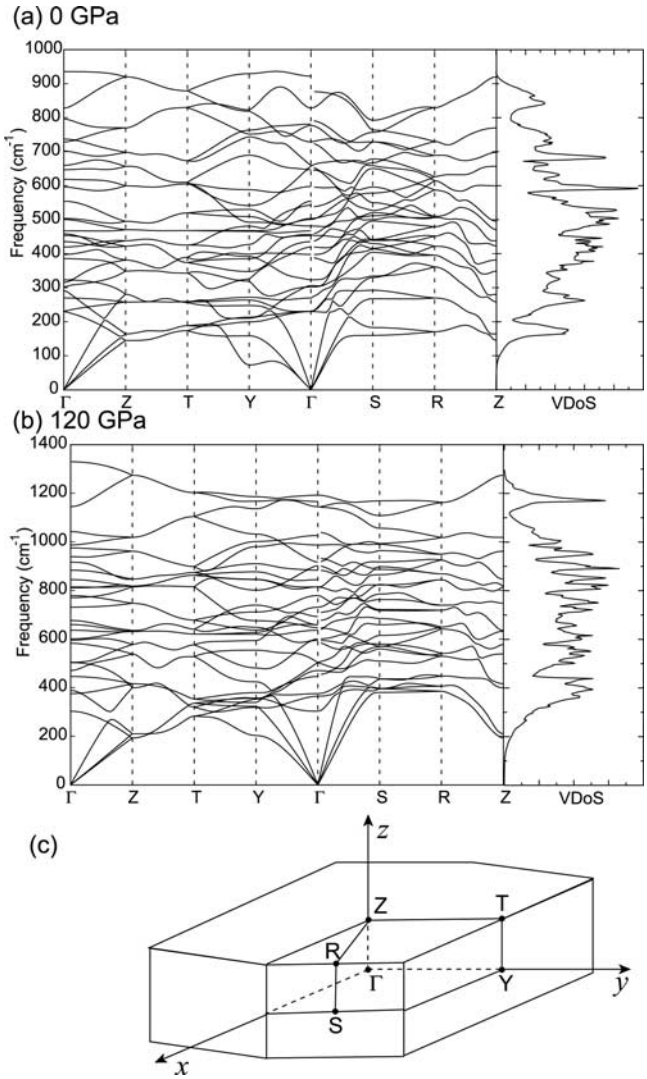

Figure 1. Phonon dispersions and vibrational density of states for $MgSiO_3$ postperovskite at (a) 0 and (b) 120 GPa. Coordinates of points on the surface of the Brillouin zone are Γ = (0 0 0), Z = (0 0 π/c), T = (0 $2\pi/b$ π/c), Y = (0 $2\pi/b$ 0), S = (π/a π/b 0), R = (π/a π/b π/c).

defined, i.e., the structure appears to be still mechanically stable, at very low temperatures at least. The combined behavior of phonons and of Born criteria is quite similar to that of ice VIII [*Umemoto and Wentzcovitch*, 2004] which can be quenched metastably at 80 K. Only when heated to 130 K, i.e., to the temperature typical of the lowest acoustic phonon branch, it amorphizes.

[14] Experimentally, postperovskite appears to amorphize under decompression at ambient conditions (K. Hirose, private communication, 2004). This is consistent with our results. Therefore our results suggest that at cryogenic temperatures postperovskite may be retrieved metastably at 0 GPa. This might be useful for investigating its unusual elastic properties, for instance.

3.3. Thermodynamical Properties

[15] When the volume dependence of the thermal energy is represented within the quasiharmonic approximation (QHA), the Helmholtz free energy takes the following form:

$$F(V,T) = U_0(V) + \frac{1}{2}\sum_{\mathbf{q},j} h\omega_j(\mathbf{q},V) + k_B T \sum_{\mathbf{q},j} \ln\left[1 - \exp\left(-h\omega_j(\mathbf{q},V)/k_B T\right)\right], \quad (7)$$

where the first, second and third terms are the static lattice, zero-point and thermal contributions, respectively. This approximation neglects the temperature dependence of phonon frequencies.

[16] A series of isotherms obtained by fitting finite temperature equation of state to the calculated free energy versus volume at various temperatures is shown in Figure 3. The volumes of the postperovskite phase are always smaller than the perovskite phase's at the same P, T conditions [*Tsuchiya et al.*, 2004a]. Thermal properties are then derived from these isothermal equations of state using standard thermodynamic relations. Several of these properties in postperovskite are compared with those of perovskite in Table 1. There are no available experimental postperovskite data for comparison but extensive and successful comparison for the perovskite phase has already been published [*Karki et al.*, 2000a].

[17] The coefficient of thermal expansion,

$$\alpha = \frac{1}{V}\left[\frac{\partial V}{\partial T}\right]_P \quad (8)$$

is determined from the temperature dependence of volume at each pressure (Figure 4b). At zero pressure, the predicted temperature dependence of α appears to be significantly biased by the QHA leading to unusually large values at very high temperatures. As pressure rises, α rapidly decreases at each temperature, and also the effects of temperature are increasingly suppressed, thus converging to a nearly constant value in the limit of high pressure and high temperature. At lower pressure, the thermal expansion coefficient of perovskite is quite smaller than postperovskite's. The difference between perovskite and postperovskite decreases

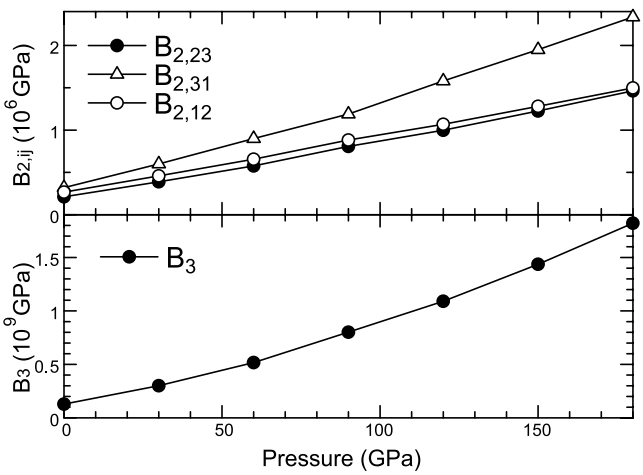

Figure 2. Pressure dependence of the Born coefficients.

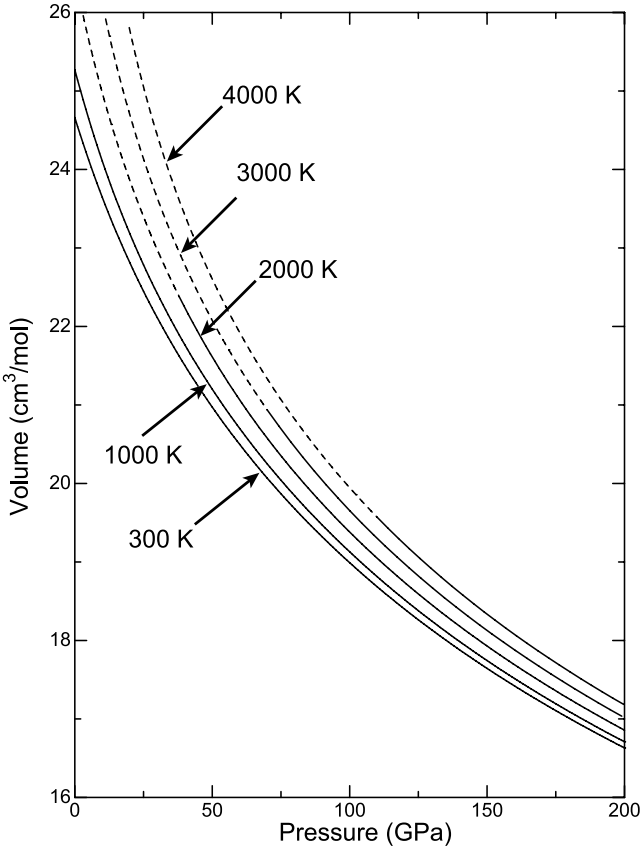

Figure 3. Pressure-volume equations of state for the static lattice and 300, 1000, 2000, 3000, and 4000 K isotherms.

with increasing pressure. Above 100 GPa, α of perovskite and of postperovskite are nearly the same.

[18] Because of the expected high temperatures in the mantle, the validity of QHA is often questioned. However, it should be valid up to some temperature between the Debye temperature (Θ_D) and the melting temperature (T_M), the latter being considerably higher than expected mantle temperatures. The calculations of thermal properties of MgO [*Karki et al.*, 2000b] and $MgSiO_3$ [*Wentzcovitch et al.*, 2004a] have indicated that the QHA is valid for these phases throughout the lower mantle regime.

[19] A posteriori inspection of their thermal expansivities, $\alpha(T)|_P$, offers a criterion for the QHA validity domain. Experimentally $\alpha\ (T)|_P$ displays linear behavior at high T's but the QHA introduces an unphysical divergence after some inflection point at $T = T_I(P)$. We take $T_I(P)$ as the upper limit for which our results should be considered predictive. This criterion indicates the QHA is valid for perovskite and postperovskite within the P, T regime of the lower mantle (Figure 5), except perhaps at the top of the lower mantle, i.e., at $P = 23$ GPa and $T \approx 1900 \sim 2000$ K. On the basis of this criterion alone, the valid temperature and pressure conditions of the QHA for postperovskite appears to be similar to that of perovskite.

[20] This criterion appears to be quite strict for the free energies themselves, but perhaps not sufficiently strict for quantities involving temperature derivatives such as the constant volume specific heat, C_V, α, etc. The thermal Grüneisen parameter,

$$\gamma_{\text{th}} = \frac{\alpha V K_T}{C_V}, \tag{9}$$

may be particularly sensitive to this approximation since it involves two temperature derivative quantities, α and C_V. Below 30 GPa, postperovskite's γ_{th} increases rapidly, and so does its temperature dependence. This behavior seems anomalous and might be caused by the inadequacy of the QHA for this quantity in this regime.

[21] The specific heat at constant pressure (C_P) calculated from $C_P = C_V(1 + \alpha\gamma T)$ and the entropy (S) are shown in Figures 4d and 4f, respectively. The difference between C_V of perovskite and postperovskite are rather negligible at each pressure (Figure 4e). The entropy S of postperovskite is slightly smaller than that of perovskite at stable pressure conditions giving a Clapeyron slope, $dP_T/dT = \Delta S/\Delta V \sim 7.5$ MPa/K for the postperovskite transition.

[22] The thermodynamic properties reported here are significant inputs for geodynamic modeling. Our calculations indicate that the thermal expansivity, specific heat,

Table 1. Thermodynamical Parameters of $MgSiO_3$ Postperovskite and Perovskite Within the Quasi-harmonic Approximation[a]

	0 GPa		100 GPa							
	300 K		300 K		1000 K		2000 K		3000 K	
V, cm^3/mol	24.66	(24.71)	18.99	(19.28)	19.13	(19.42)	19.38	(19.67)	19.65	(19.95)
B_T, GPa	215.9	(246.1)	598.1	(599.2)	582.5	(584.2)	558.2	(560.8)	533.0	(536.7)
$\partial B_T/\partial P$	4.41	(4.00)	3.48	(3.24)	3.52	(3.28)	3.60	(3.34)	3.68	(3.40)
α, $\times 10^{-5}$ K^{-1}	2.57	(2.19)	0.62	(0.62)	1.23	(1.23)	1.36	(1.36)	1.43	(1.43)
γ	1.68	(1.61)	1.18	(1.19)	1.20	(1.22)	1.21	(1.23)	1.22	(1.24)
S, J/mol K	58.6	(59.0)	32.7	(35.1)	145.5	(147.7)	230.0	(232.2)	281.9	(284.1)
	125 GPa									
	300 K		1000 K		2000 K		3000 K		4000 K	
V, cm^3/mol	18.26	(19.28)	18.38	(19.42)	18.59	(19.67)	18.82	(19.95)	19.06	(19.35)
B_T, GPa	683.8	(679.1)	669.1	(665.2)	646.4	(643.3)	623.0	(620.5)	598.9	(597.1)
$\partial B_T/\partial P$	3.38	(3.15)	3.41	(3.20)	3.46	(3.26)	3.53	(3.31)	3.60	(3.36)
α, $\times 10^{-5}$ K^{-1}	0.52	(0.53)	1.08	(1.09)	1.20	(1.20)	1.25	(1.26)	1.30	(1.31)
γ	1.14	(1.16)	1.17	(1.19)	1.18	(1.20)	1.19	(1.21)	1.20	(1.22)
S, J/mol K	30.0	(32.4)	140.1	(142.2)	223.9	(226.0)	275.5	(277.6)	313.0	(315.1)

[a]Values in parentheses are for perovskite.

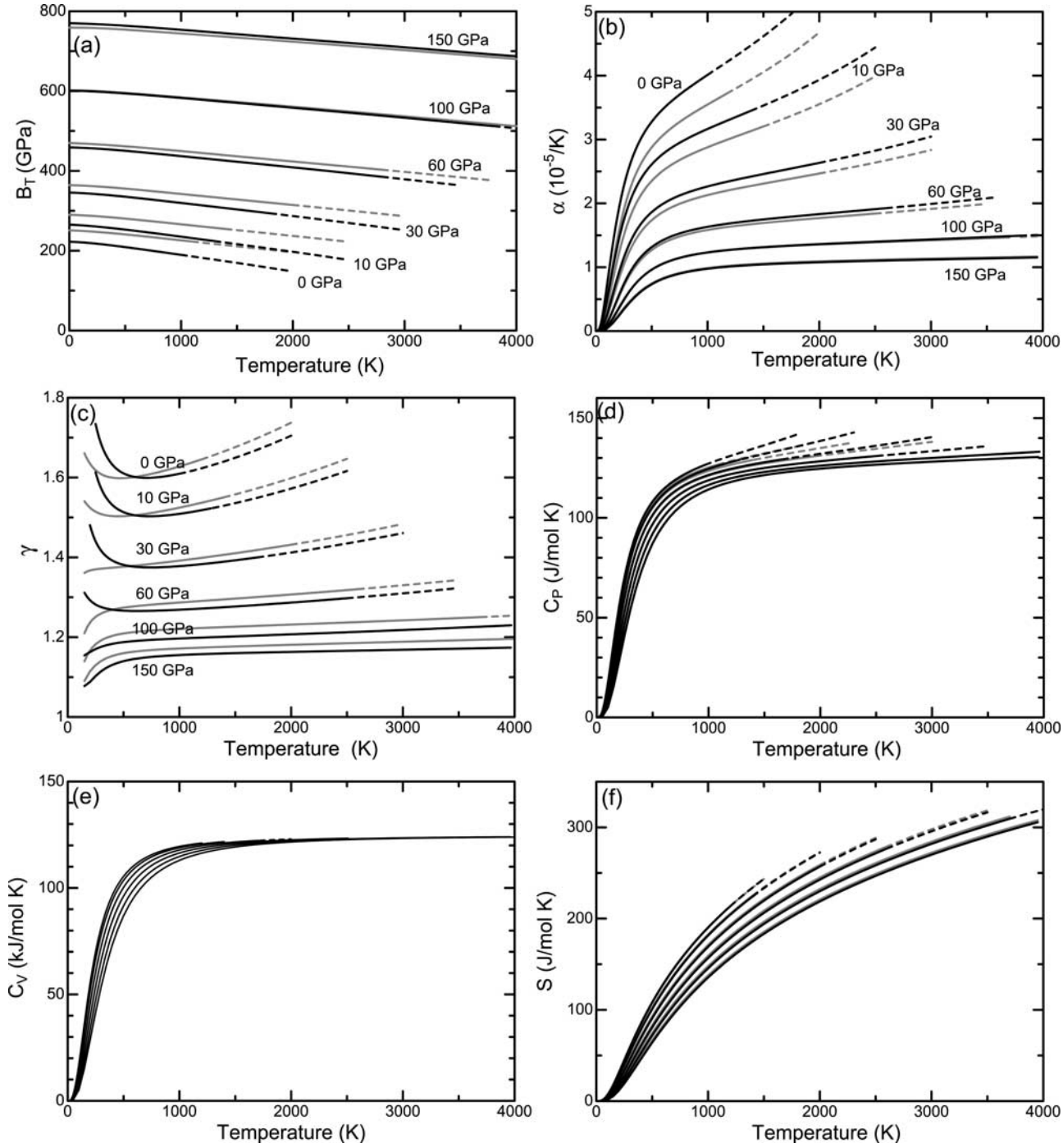

Figure 4. (a–c) Isothermal bulk modulus B_T, coefficients of thermal expansion α and Grüneisen parameter γ of perovskite and postperovskite at 0, 10, 30, 60, 100, and 150 GPa. Black and gray lines indicate the thermodynamic properties of postperovskite and perovskite, respectively. (d–f) Temperature dependence of heat capacity C_P, C_V, and entropy S along the isobars at 0, 10, 30, 60, 100, and 150 GPa (solid lines from top to the bottom).

thermal Grüneisen parameter etc., change very little across the postperovskite transition. Although it has been pointed out that small changes in thermal expansivity lead to significant variations in mantle convection pattern and its time evolution [*Ita and King*, 1998], it appears that the changes here are quite insignificant for such effects to happen. The major effects of a postperovskite transition on the dynamics at the bottom of the lower mantle have already been investigated and reported by *Nakagawa and Tackley* [2004]. This exothermic transition with a large and positive Clapeyron slope enhances mantle convection and raises the overall mantle geotherm by ~200 K. Determining the changes in rheological properties across the transformation is now the key issue for assessing the effects

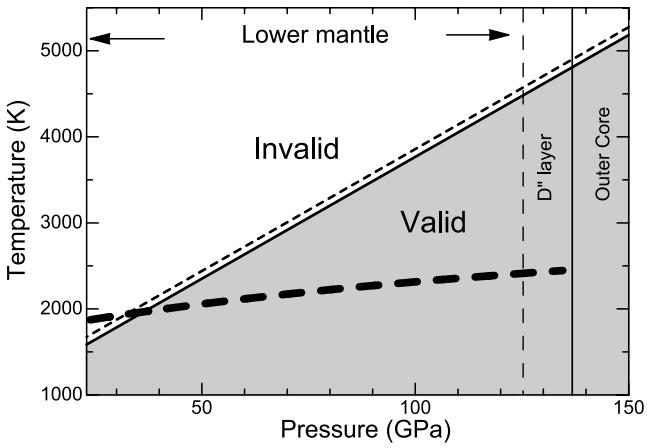

Figure 5. The valid *P*, *T* region of QHA. The solid and dashed lines show the valid range of postperovskite and perovskite, respectively. Thick dashed line indicates the *Brown and Shankland* [1981] mantle geotherm.

of such transformation more realistically. Obviously, effects of minor elements (Al, Fe) partitioning on all properties across the transition also must be considered. This fact might be of minor significance considering that the D″ region is a thermochemical boundary layer with strong heterogeneities.

4. Summary

[23] We have calculated ab initio phonon dispersion and vibrational density of states of $MgSiO_3$ postperovskite, the new high-pressure phase of perovskite, up to 180 GPa using density functional perturbation theory. Several thermodynamical quantities of interest have been derived within the quasi-harmonic approximation. The overall thermodynamic properties of postperovskite are almost the same as those of perovskite within its thermodynamic stability field and the values of these properties are important inputs for geodynamic modeling. Finally, it appears that postperovskite may be retrieved metastably to ambient pressures or nearly so, at cryogenic temperatures.

[24] **Acknowledgments.** This research was supported by NSF/EAR 0135533 and 0230319 and NSF/ITR 0428774. J.T. acknowledges the Japan Society for the Promotion of Science (JSPS) for research fellowships.

References

Baroni, S., P. Giannozzi, and A. Testa (1987), Green's function approach to linear response in solids, *Phys. Rev. Lett.*, *58*, 1861–1864.

Baroni, S., S. de Gironcoli, A. Dal Corso, and P. Giannozzi (2001), Phonons and related crystal properties from density-functional perturbation theory, *Rev. Mod. Phys.*, *73*, 515–562.

Born, M., and K. Huang (1954), *Dynamical Theory of Crystal Lattices*, 432 pp., Oxford Univ. Press, New York.

Brown, J. M., and T. J. Shankland (1981), Thermodynamic parameters in the Earth as determined from seismic profiles, *Geophys. J. R. Astron. Soc.*, *66*, 579–596.

Ceperley, D. M., and B. J. Alder (1980), Ground state of the electron gas by a stochastic method, *Phys. Rev. Lett.*, *45*, 566–569.

Chaplot, S. L., and S. K. Sikka (1993), Comment on "Elastic instability in α-quartz under pressure," *Phys. Rev. Lett.*, *71*, 2674.

Hirose, K., K. Kawamura, Y. Ohishi, S. Tateno, and N. Sata (2004), Stability and equation of state of $MgGeO_3$ post-perovskite phase, *Am. Mineral.*, *90*, 262–265.

Hohenberg, P., and W. Kohn (1964), Inhomogeneous electron gas, *Phys. Rev.*, *136*, B364–B871.

Hyde, B. G., and S. Anderson (1989), *Inorganic Crystal Structures*, 430 pp., Wiley-Interscience, New York.

Iitaka, T., K. Hirose, K. Kawamura, and M. Murakami (2004), The elasticity of the $MgSiO_3$ post-perovsktie phase in the Earth's lowermost mantle, *Nature*, *430*, 442–445, doi:10.1038/nature02702.

Ita, J., and S. D. King (1998), The influence of thermodynamic formulation on simulations of subduction zone geometry and history, *Geophys. Res. Lett.*, *25*, 1463–1466.

Karki, B. B., R. M. Wentzcovitch, S. de Gironcoli, and S. Baroni (2000a), *Ab initio* lattice dynamics of $MgSiO_3$ perovskite at high pressure, *Phys. Rev. B*, *62*, 14,750–14,756.

Karki, B. B., R. M. Wentzcovitch, S. de Gironcoli, and S. Baroni (2000b), High-pressure lattice dynamics and thermoelasticity of MgO, *Phys. Rev. B*, *61*, 8793–8800.

Karki, B. B., R. M. Wentzcovitch, S. de Giuroncoli, and S. Baroni (2001), High-pressure elastic properties of major materials of earth's mantle from first principles, *Geophys. Res. Lett.*, *28*, 2699–2702.

Monkhorst, H. J., and J. D. Pack (1976), Special points for Brillouin-zone integrations, *Phys. Rev. B*, *13*, 5188–5192.

Murakami, M., K. Hirose, K. Kawamura, N. Sata, and Y. Ohishi (2004), Post-perovskite phase transition in $MgSiO_3$, *Science*, *304*, 855–858, doi:10.1126/science.1095932.

Nakagawa, T., and P. J. Tackley (2004), Effects of a perovskite-post perovskite phase change near core-mantle boundary in compressible mantle convection, *Geophys. Res. Lett.*, *31*, L16611, doi:10.1029/2004GL020648.

Oganov, A. R., and S. Ono (2004), Theoretical and experimental evidence for a post-perovskite phase of $MgSiO_3$ in Earth's D″ layer, *Nature*, *430*, 445–448, doi:10.1038/nature02701.

Perdew, J. P., and A. Zunger (1981), Self-interaction correction to density-functional approximations for many-electron systems, *Phys. Rev. B*, *23*, 5048–5079.

Troullier, N., and J. L. Martins (1991), Efficient pseudopotential for plane wave calculations, *Phys. Rev. B*, *43*, 1993–2006.

Tsuchiya, T., J. Tsuchiya, K. Umemoto, and R. M. Wentzcovitch (2004a), Phase transition in $MgSiO_3$ perovskite in the Earth's lower mantle, *Earth Planet. Sci. Lett.*, *224*, 241–248, doi:10.1016/j.epsl.2004.05.017.

Tsuchiya, T., J. Tsuchiya, K. Umemoto, and R. M. Wentzcovitch (2004b), Elasticity of post-perovskite $MgSiO_3$, *Geophys. Res. Lett.*, *31*, L14603, doi:10.1029/2004GL020278.

Tsuchiya, T., R. Caracas, and J. Tsuchiya (2004c), First principles determination of the phase boundaries of high-presusre polymorphs of silica, *Geophys. Res. Lett.*, *31*, L11610, doi:10.1029/2004GL019649.

Umemoto, K., and R. M. Wentzcovitch (2004), Anomalous pressure-induced transition(s) in Ice XI, *Phys. Rev. Lett.*, *92*, 105502, doi:10.1103/PhysRevLett.92.105502.

Wentzcovitch, R. M., B. B. Karki, M. Cococcioni, and S. de Gironcoli (2004), Thermoelastic properties of $MgSiO_3$-perovskite: Insights on the nature of the Earth's lower mantle, *Phys. Rev. Lett.*, *92*, 018501, doi:10.1103/PhysRevLett.92.018501.

Wentzcovitch, R. M., L. Stixrude, B. B. Karki, and B. Kiefer (2004), Akimotite to perovskite phase transition in $MgSiO_3$, *Geophys. Res. Lett.*, *31*, L10611, doi:10.1029/2004GL019704.

J. Tsuchiya, T. Tsuchiya, and R. M. Wentzcovitch, Department of Chemical Engineering and Materials Science, Minnesota Supercomputing Institute for Digital Technology and Advanced Computation, University of Minnesota, 421 Washington Avenue SE, Minneapolis, MN 55455, USA. (junt@cems.umn.edu)